LAWRENCE
LIVERMORE
NATIONAL
LABORATORY

UCRL-CONF-207379

Suppression of Large Edge Localized Modes with a Stochastic Magnetic Boundary in High Confinement DIII-D Plasmas

T. E. Evans, R. A. Moyer, J. G. Watkins, T. H. Osborne, P. R. Thomas, M. Becoulet, J. A. Boedo, E. J. Doyle, M. E. Fenstermacher, K. H. Finken, R. J. Groebner, M. Groth, J. H. Harris, G. L. Jackson, R. J. La Haye, C. J. Lasnier, S. Masuzaki, N. Ohyabu, D. G. Pretty, H. Reimerdes, T. L. Rhodes, D. L. Rudakov, M. J. Schaffer, M. Wade, G. Wang, W. P. West, L. Zeng

October 20, 2004

20th IAEA Conference
Vilamoura, Portugal
November 1, 2004 through November 6, 2004

Suppression of Large Edge Localized Modes with a Stochastic Magnetic Boundary in High Confinement DIII–D Plasmas*

T.E. Evans 1), R.A. Moyer 2), J.G. Watkins 3), T.H. Osborne 1), P.R. Thomas 4), M. Becoulet 4) J.A. Boedo 2), E.J. Doyle 5), M.E. Fenstermacher 6), K.H. Finken 7), R.J. Groebner 1), M. Groth 6), J.H. Harris 8), G.L. Jackson 1), R.J. La Haye 1), C.J. Lasnier 6), S. Masuzaki 9), N. Ohyabu 9), D.G. Pretty 8), H. Reimerdes 10), T.L. Rhodes 5), D.L. Rudakov 2), M.J. Schaffer 1), M. Wade 11), G. Wang 5), W.P. West 1), and L. Zeng 5)

1) General Atomics, San Diego, California, 92186 U.S.A.
2) University of California San Diego, La Jolla, California, U.S.A.
3) Sandia National Laboratory, Albuquerque, New Mexico, U.S.A.
4) CEA Cadarache Euratom Association, Cadarache, France
5) University of California, Los Angeles, California, U.S.A.
6) Lawrence Livermore National Laboratory, Livermore, California, U.S.A.
7) FZ-Julich Euratom Association, Julich, Germany
8) Australian National University, Canberra, Australia
9) National Institute for Fusion Science, Gifu-ken, Japan
10) Columbia University, New York, New York, U.S.A.
11) Oak Ridge National Laboratory, Oak Ridge, Tennessee, U.S.A.

email: evans@fusion.gat.com

Abstract. Large sub-millisecond heat pulses due to Type-I ELMs have been reproducibly eliminated in DIII–D for periods approaching 7 energy confinement times with small dc currents driven in a simple magnetic perturbation coil. The current required to eliminate all but a few isolated Type-I ELM impulses during a perturbation coil pulse lasting several seconds is less than 0.4% of plasma current. Based on vacuum magnetic field line modeling, perturbation fields from the coil resonate strongly with plasma flux surfaces across most of the pedestal region ($0.9 \le \psi_N \le 1.0$) when $q_{95} = 3.7 \pm 0.2$ creating small remnant magnetic islands surrounded by weakly stochastic field lines. Under the best ELM suppression conditions, the stored energy, β_N and H–mode quality factor are unaffected by the perturbation field along with the electron pressure profile, radial electric field and poloidal rotation across the pedestal. Consequently, the H–mode transport barrier and global energy confinement time is also unaltered in these cases. Although some isolated ELM-like events typically occur during the perturbation coil pulse, long periods free of large Type-I ELMs ($\Delta t > 4–6\ \tau_E$) have been reproduced numerous times, on multiple experimental run days. Several Type-I ELM suppression and modification behaviors have been identified and studied over a range of discharge conditions including those matching the ITER scenario 2 flux surface shape and aspect ratio scaled down by a factor of 3.5 to fit in the DIII–D vacuum vessel. Since large Type-I ELM impulses represent a severe constraint on the survivability of the divertor target plates in future fusion devices such as ITER, a proven method of eliminating these impulses is critical for the development of tokamak reactors. Results presented in this paper suggest that non-axisymmetric edge magnetic perturbations could be a promising option for controlling ELMs in future tokamaks such as ITER.

1. Introduction

Edge localized modes (ELMs) are repetitive instabilities that often appear in the pedestal region of plasmas with edge transport barriers (H–mode plasmas). While these instabilities play an important role in regulating the global confinement and core impurity content of the plasma, they are also expected to pose a significant threat to the integrity of plasma facing materials as the energy content of the plasma approaches reactor relevant conditions [1]. In their most severe form, Type-I ELMs produce a rapid loss of energy from the pedestal region that is known to result in large impulsive loads on divertor target plates. In future tokamaks, thermal impulses due to Type-I ELMs are expected to significantly exceed the 45 MJ • m^{-2} $s^{-1/2}$ [2] ablation threshold limit of carbon divertor tiles.

Because of their potential for eroding divertor target plates in high power discharges, Type-I ELMs must be controlled in fusion reactors such as ITER [3]. The control method used must be capable of reducing the amplitude of energy impulses without significantly altering the pressure at the top of the pedestal. It must also be capable of replacing the impulsive thermal and particle transport (thermal electrons and deuterium as well as impurity ions) driven by Type-I ELMs with a more benign mechanism (i.e., a lower amplitude, longer duration transport process) in order to avoid an uncontrolled increase in the core density or a detrimental accumulation of the impurity ions in the core plasma. Several prospective types of steady-state control techniques are being examined in the current generation of tokamaks including: (1) impurity seeding [4], (2) the injection of small pellets to trigger ELM-like events (i.e., ELM pace-making) [5], and (3) the use of resonant magnetic perturbations (RMPs) [6–9]. In this paper we focus on recent results using RMPs in DIII–D.

2. Experimental Overview and Results

Dedicated Type-I ELM control experiments using edge RMPs were initiated in 2003 on DIII–D. Beginning with the 2003 operations period, DIII–D was equipped with a set of internal MHD control coils designed specifically for $n=1$ resistive wall mode (RWM) feedback control experiments. Field line integration modeling of $n=3$ perturbations from these coils with the TRIP3D code [10] showed that they are also reasonably well suited for producing modest edge stochastic layers with relatively small core perturbations, so-called clean stochastic boundary layers [8]. In DIII–D the first application of these clean stochastic boundaries was in the area of Type-I ELM control.

Based on linear ELM stability theory, small changes in the pedestal pressure and current profiles can have a significant stabilizing effect on large Type-I ELMs. Thus, the goal of the DIII–D edge stochastic layer experiments is to enhance the heat and particle transport across the outer part of the pedestal, locally decrease the electron temperature gradient and flatten the pressure profile while enhancing the line radiation from this region. In addition to modifying the pressure and bootstrap current profiles, this is expected to produce a cold buffer plasma surrounding the pedestal. Assuming the edge transport barrier is unaltered and the pressure profile shifts somewhat inward without a significant increase in gradient, this should have a stabilizing effect on Type-I ELMs and produce smaller amplitude structures with higher frequencies similar to the more benign Type-II ELMs. Additionally, the buffer plasma provides a steady-state mechanism that radiatively spreads the energy flux escaping from the pedestal over a broad area of the divertor targets and wall. This serves to mitigate any remaining heat pulses that escape from the hot plasma region confined within the buffer layer.

A variety of ELM suppression and modification results, over a range of plasma shapes and conditions, have been obtained during these experiments in DIII–D. Our best case suppression results are quite interesting from a physics prospective because they leave the electron pressure profile essentially unaltered, along with the energy confinement time, the radial electric field and the poloidal rotation profile. At the same time, the C VI ion pressure profile gradient increases and is shifted outward while both the edge and core toroidal rotation drops significantly. Under the best conditions for Type-I ELM suppression, the data does not support the original expectation that enhanced transport at the foot of the pedestal flattens the pressure profiles and thus modify the peeling-ballooning stability threshold. This is most likely due to the fact that the I-coil was not specifically designed to produce well controlled, edge localized, stochastic boundary layers (the poloidal mode spectrum is marginally suitable for this application) and during its initial operations phase has been limited to coil currents of 4.4 kA or less. Although the best ELM suppression cases appear to result from an unanticipated stabilization mechanism, we also find that changes in perturbation coil configuration can produce a plasma response that is in relatively good agreement with the effects expected to be produced by a broader edge stochastic layer including an increase in the midplane recycling and an unambiguous flattening of the electron and C VI ion pressure profiles. In these cases, some Type-I ELM suppression is observed but because of the I-coil

current operational limit, this regime has not been fully explored. In this paper, we give a description of the perturbation coil configuration and discharge conditions used for best case Type-I ELM suppression results (when run in a reference discharge shape) and compare these results with those obtained in an ITER scenario 2 shape.

2.1. Description of the resonant magnetic perturbation coil

The RWM control coil mounted inside the DIII–D vacuum vessel, referred to as the I-coil [11], is used as a controlled perturbation field source for the ELM suppression experiments. The 3D geometry of the I-coil is shown in Fig. 1. Since the C-coil, used to correct measured field errors on the $m,n = 2,1$ surface, is known to perturb both the core and pedestal plasma [12] it was turned off for these experiments.

In order to minimize core RMPs due to the I-coil, toroidally adjacent segments are driven with opposite polarities producing an $n = 3$ toroidal mode structure. A poloidal m=12±3 mode structure is used for edge resonant studies. Positive current is defined to be in the counter-clockwise direction as viewed inward toward the toroidal axis and the corresponding perturbation field (δB) points in the direction of positive major radius R (see the upper segment at 210 deg in Fig. 1). The up/down parity of the coil is referred to as "odd" when the upper and lower coil segments have opposite polarities at each toroidal angle ϕ and the toroidal phase angle $\phi_{\mathrm{I-coil}} = 0$ deg is defined by a positive current in the upper 30 deg segment.

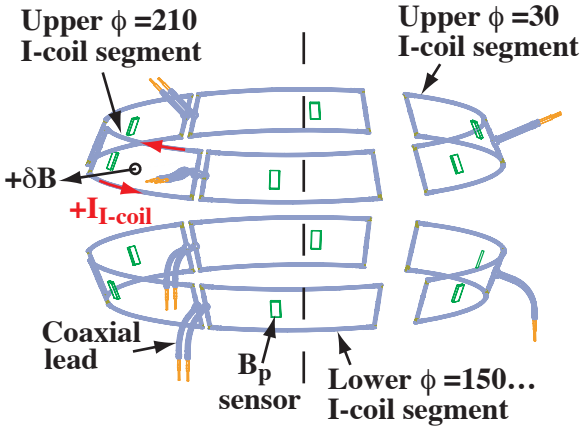

FIG. 1. The DIII–D I-coil is comprised of six segments above the equatorial plane (upper) and six segments below the equatorial plane (lower) centered at 60 deg toroidal angle (ϕ) increments (starting at 30 deg).

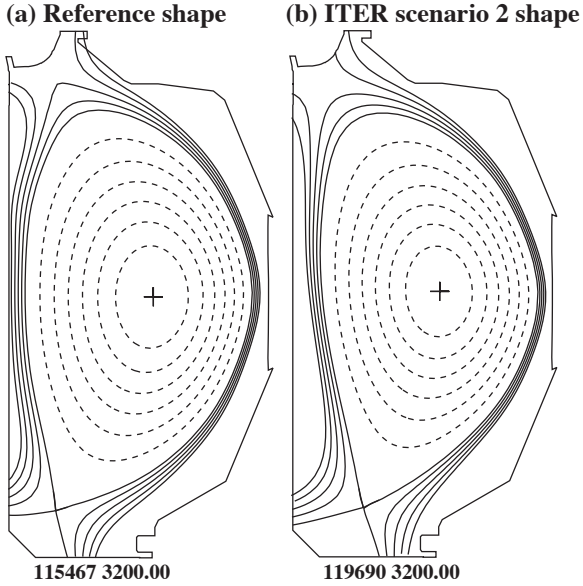

FIG. 2. Comparison between DIII–D ELM suppression shapes for discharges (a) 115467 reference shape and (b) 119690:ITER scenario 2 shape.

2.2. Description of discharge types

Results from two types of plasma configurations are discussed in this paper. The first is the reference ELM suppression configuration having a modestly up-down asymmetric equilibrium biased downward by 2.0 cm. This shape, shown in Fig. 2(a), has an elongation (κ) of 1.8, upper (δ_{up}) and lower (δ_{low}) triangularities of 0.35 and 0.73 respectively, a toroidal magnetic field $B_{\mathrm{T}} = 1.6$ T, a plasma current $I_{\mathrm{p}} = 1.1$ MA, neutral beam heating power (P_{NBI}) of 5.1 MW and an aspect ratio (A) of 3.1. In these discharges, the line averaged electron density (n_{e}) was 6.94×10^{19} m^{-3} with $\beta_{\mathrm{N}} = 2.3$, $H_{\mathrm{L89}} = 2.1$, $\tau_{\mathrm{E}} = 163$ ms, a stored energy of 0.71 MJ and a safety factor at the 95% flux surface (q_{95}) of 3.8. The second configuration, shown in Fig. 2(b), is derived from an ITER eqdsk file provided by the ITER team [13] that is scaled down by a factor of 3.5 to fit into the DIII–D vacuum vessel. These plasmas have an elongation (κ) of 1.8, upper (δ_{up}) and lower (δ_{low}) triangularities of 0.43 and 0.60 respectively, a toroidal magnetic field $B_{\mathrm{T}} = 1.6$ T, a plasma current $I_{\mathrm{p}} = 1.0$ MA, neutral

beam heating power (P_{NBI}) of 4.8 MW and an aspect ratio (A) of 3.1. In these discharges, the line averaged electron density (n_e) was 7.24×10^{19} m^{-3} with $\beta_N = 2.0$, $H_{L89} = 1.9$, $\tau_E = 163$ ms, a stored energy of 0.57 MJ and a safety factor at the 95% flux surface (q_{95}) of 3.7.

The time evolution of I_p, P_{NBI}, n_e, the D_2 gas fueling and the I-coil pulse ($I_{coil} = 4.4$ kA) is shown for a reference ELM suppression configuration (discharge 115467) and for an ITER scenario 2 configuration (discharge 119690) in Fig. 3. Reproducible ELM suppression has also been obtained in the reference configuration with $B_T = 2.0$ T and $I_p = 1.4$ MA ($q_{95} = 3.8$) as well as with $B_T = 2.0$ T and $I_p = 1.1$ MA ($q_{95} = 4.9$).

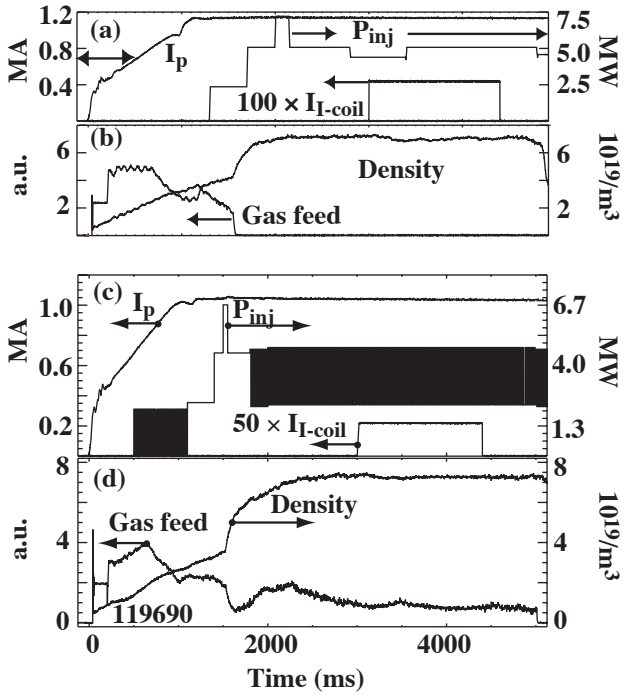

FIG. 3. Temporal evolution of (a) I_p, P_{inj}, the I_{I-coil} current, (b) the D_2 gas fueling, n_e in discharge 115467 and temporal evolution of (c) I_p, P_{inj}, (modulation shown as thick black regions) the I_{I-coil} current, (d) the D_2 gas fueling and n_e in discharge 119690 (the ITER scenario 2 shape).

2.3. Experimental results

A notable characteristic of good ELM suppression with $n=3$ I-coil perturbations is a global change in the dynamics of the D_α recycling light measured at various toroidal and poloidal locations. Well correlated changes in all the divertor diagnostic typically used to monitor the properties of the ELMs are also seen. An example of the change seen in the divertor D_α ELM dynamics when the I-coil is applied to a discharge in the reference configuration is shown in Fig. 4. Here, a discharge with an $n=3$ I-coil pulse (115467) is compared to a reference discharge without an I-coil pulse (115468). Identical changes are also observed in the midplane D_α signals at $\phi = 45$ deg, all of the lower divertor D_α signals at $\phi = 135$ deg, all of the upper divertor D_α signals at $\phi = 150$ deg, the inner wall D_α at $\phi = 135$ deg and the lower divertor surface temperature measured by an IRTV at $\phi = 165$ deg. Changes consistent with Type-I ELM suppression are also seen in the core B_{dot} signals at the outer midplane, $\phi = 322$ deg, and in the edge B_{dot} signal from the divertor at $\phi = 322$ deg. Fixed Langmuir probes in the lower divertor at $\phi = 180$ deg, measuring ion saturation current, also see a reduction in the particle flux consistent with the suppression of Type-I ELMs during the I-coil pulse.

Each of these diagnostics show three well defined characteristics during the ELM suppression phase. Large spikes due to Type-I ELMs are suppressed within a single 15 ms ELM period, small 130 Hz coherent oscillations with a 2 ms quiet period and a 6 ms active period are observed between intermittent Type-I ELM-like events and when the perturbation field is turned off large Type-I ELMs return with properties very similar to those before the perturbation pulse. When the I-coil current is first switched on at $t = 3000$ ms there is a short $\Delta t \sim 20$–30 ms period of small incoherent fluctuations. Although this activity looks remarkably similar to the behavior seen in the discharge without the I-coil pulse (115468), large Type-I ELMs are immediately suppressed. A first indication of the onset of coherent oscillations is observed at ~3040 ms and intermittent Type-I ELM-like events such as the one shown at $t = 3243$ ms sometimes punctuate the oscillations. Note that the oscillations become rather chaotic after the isolated event but eventually recover their coherent structure.

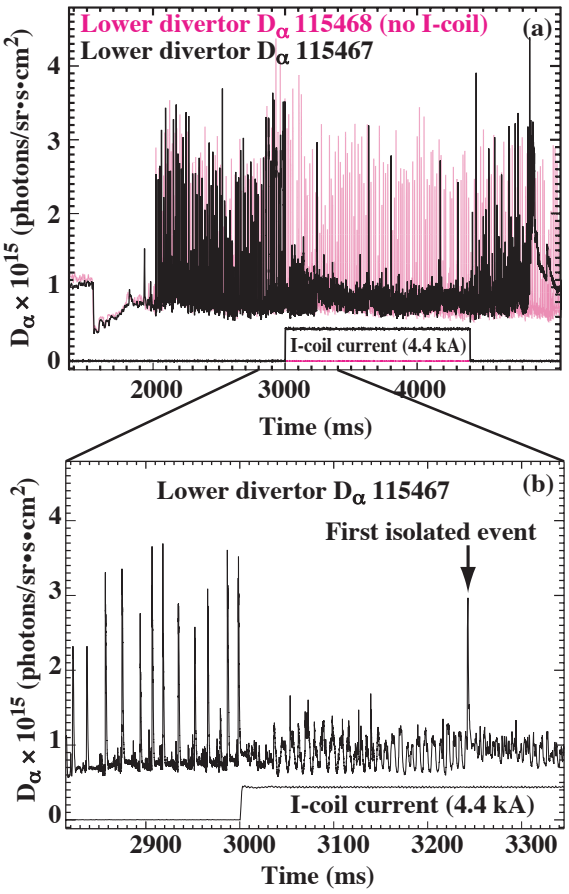

FIG. 4. (a) Lower divertor D_α signal near the outer strike point showing Type-I ELM suppression in discharge 115467 (black) during an $I_{\text{I-coil}}$ current pulse of 4.4 kA starting at t_{on} = 3000 ms and ending at t_{off} = 4400 ms compared to an identical discharge, 115468 (magenta), without an I-coil current pulse. (b) A shorter time window showing a change in the dynamics across the I-coil turn on time.

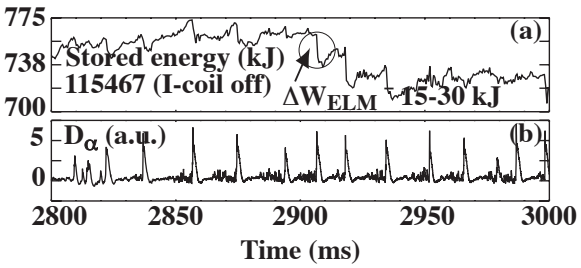

FIG. 5. (a) The stored energy showing changes associated with each ELM, (no I-coil current). (b) A lower divertor D_α signal (100 μs resolution).

Subsequent isolated events have similar effects on the oscillations. Near the foot of the pedestal the toroidal rotation, which has been dropping since the I-coil current was switched on, reaches zero at roughly the same time as these oscillations first appear. Deeper inside the plasma, well inside the pedestal region, the toroidal rotation drops on a slower time scale reaching approximately one-third its initial value without the I-coil perturbation by t = 3300 ms.

A key feature of the coherent oscillations is that they appear to result from a process that produces about the same time averaged transport through the pedestal as is seen during the Type-I ELMing phase but without the large impulsive component typical of the Type-I ELMs. This is attributed to the longer active period and smaller amplitudes of these structures compared to the rapid Type-I ELM spikes. Similar effects are observed in the stored energy calculated from EFIT equilibrium reconstructions with time steps of Δt_{WMHD} = 500 μs. During the ELMing phase, Type-I ELMs transport as much as 30 kJ of the pedestal energy into the scrape-off layer during one Δt_{WMHD} as shown by the largest drops in Fig. 5(a) [Fig. 5(b) shows lower divertor D_α spikes associated with drops in the stored energy]. Several midplane diagnostics indicate that this energy is expelled over a timeframe approaching 200 μs or less. Since the magnitude of the drop can be somewhat underestimated by the Δt_{WMHD} step in the EFIT calculation, this implies a minimum impulsive source into the SOL for the largest ELMs of $E_{\text{imp}} = \Delta E_{\text{WMHD}}/t^{1/2}$ = 2.10 MJ/s$^{1/2}$. With the I-coil current turned on, the stored energy drops are considerably smaller and slower as shown in Fig. 6(a) [with the associated lower divertor D_α oscillations shown in Fig. 6(b)]. The largest of these are of order 15 kJ and evolve over periods of approximately 500 μs. Thus, the largest impulsive source into the SOL reach a maximum of E_{imp} = 0.67 × MJ/s$^{1/2}$ implying at least a factor of 3 reduction with the perturbation from the I-coil. While such estimates are informative, they do not address such key issues as how much of the energy lost from the pedestal reaches the divertor targets and main chamber walls or how the energy is distributed over these plasma facing surfaces. Our data shows that the

energy lost from the pedestal is dispersed over a larger area by the perturbed magnetic topology.

In DIII–D, fixed Langmuir probes and infrared (IR) cameras directly measure heat and particle flux to the divertor target plates due to ELM impulses. These diagnostic can be used to determine the absolute magnitudes of heat and particle flux impulses striking plasma facing surfaces that are most vulnerable to damage from Type-I ELMs. An example of this is given in Fig. 7 where fast radial line scan data from an IR camera viewing the lower DIII–D divertor is shown averaged over 5 ELM peaks [Fig. 7(a)] prior to the I-coil pulse and 4 peaks during the active phase of the 130 Hz oscillations seen during the I-coil pulse [Fig. 7(b)]. A full radial scan of the lower divertor target plates is acquired every 100 μs and those scans with peaks corresponding to Type-I ELM or the active phase of the 130 Hz oscillations are selected and averaged to produce this plot. For the I-coil off phase, Fig. 7(a), two significant peaks near the inner (R = 1.1 m) and outer (R = 1.4 m) strike points are clearly defined. A third possible peak may be present at R = 1.6 m but this feature does not substantially exceed the noise level of the camera which is typically between 1 and 2 for the arbitrary units shown in these plots. With the I-coil on, averages over the largest peaks seen during the active phase of the oscillations, Fig. 7(b), do not reveal any significant features. This data suggests that the heat flux driven by Type-I ELM is reduced by at least a factor of 5 during the I-coil pulse.

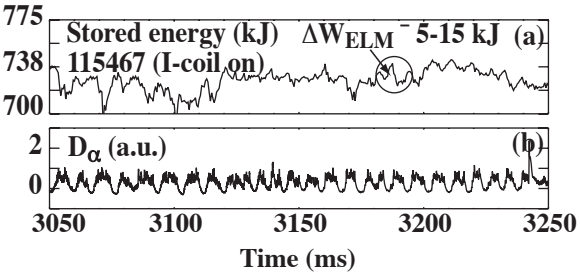

FIG. 6. (a) The fast stored energy signal as in Fig. 5(a) but during the I-coil pulse and (b) oscillations in the lower divertor D_α signal.

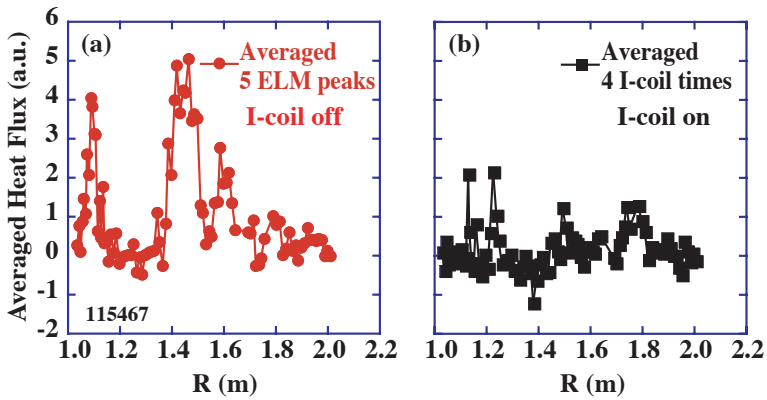

FIG. 7. (a) IRTV line scans (100 μs) of the lower divertor heat flux with the I-coil off and (b) with the I-coil on.

In general, the divertor Langmuir probes see a reduction in the impulsive particle flux (Γ_{imp}) driven by Type-I ELMs although probes at some locations see smaller reductions than others. Langmuir probe data acquired from discharges in the reference shape (115464 and 115467) show that the largest Type-I ELM driven particle flux impulses often reach $\Gamma_{imp} = \Delta\Gamma/t^{1/2} = 6.39$ kA/cm^2 s$^{1/2}$ near the outer strike point in the lower divertor. During the I-coil pulse, excluding the isolated ELM-like events discussed above, particle flux impulses are typically reduced to about 0.8 kA/cm^2 s$^{1/2}$ at the outer strike point in the lower divertor. This is a reduction in the impulsive particle flux by a factor of 8. An example of the particle flux evolution is given in Fig. 8 where an oscillation in particle flux during the I-coil pulse (black) is plotted relative to a Type-I ELM structure seen near the outer strike point before the I-coil is pulsed. For comparison, referring to the D_α signal in Fig. 5 during discharge 115467 (digitized at 100 kHz), the implied recycling impulse due to the ELM at t = 2998 ms is $D_{\alpha\_imp} = 2.99 \times 10^{16}/(60\ \mu s)^{1/2} = 3.86 \times 10^{18}$ photons/sr•cm^{2}s$^{3/2}$. This is a factor of 3.1 larger than that due to the largest feature $D_{\alpha\_imp} = 0.79 \times 10^{16}/(40\ \mu s)^{1/2} = 1.25 \times 10^{18}$ photons/sr•cm^{2}s$^{3/2}$ seen with the I-coil on.

Signals from a midplane reciprocating Langmuir probe located ~4 cm outside the unperturbed separatrix also show a suppression of the Type-I ELM impulses and an increase in higher frequency fluctuations that appear to fill in the periods between the ELM crashes

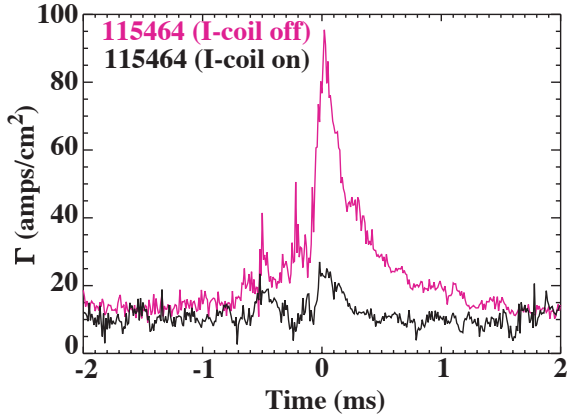

FIG. 8. A lower divertor Langmuir probe signal near the outer strike point without the I-coil (magenta) and with the I-coil (black). The impulsive particle flux to this probe is reduced by about a factor of 8.

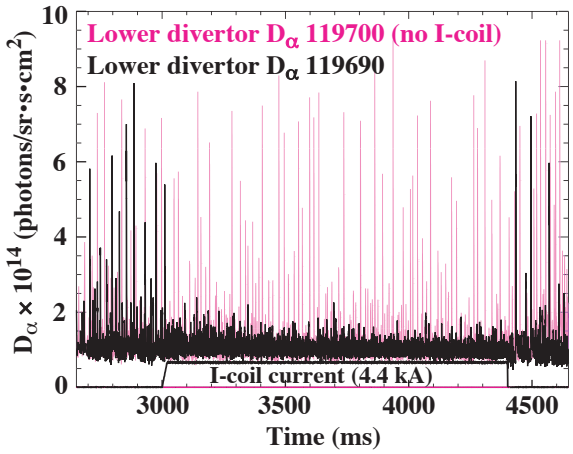

FIG. 9. Lower divertor D_α signal near the outer strike point showing Type-I ELM suppression in ITER Scenario 2 discharge 119690 (black) during an $I_{\mathrm{I-coil}}$ current pulse. Compared to an identical discharge, 119700 (magenta), without an I-coil current pulse.

prior to the I-coil pulse. The nature of these higher frequency components is still under investigation but they appear to be very similar to behavior seen in the midplane reflectometer and edge magnetic probe data and suggest that the I-coil perturbation is effectively opening up a higher frequency transport channel which moderates the buildup of the pedestal conditions needed for triggering large Type-I ELMs.

A natural question to be addressed by this line of research is its applicability to other shapes and plasma parameters. Safety factor scans (q_{95}) done while in the reference shape clearly demonstrate that the suppression mechanism involves a rather sharp resonance effect that is maximized at q_{95} = 3.7±0.2. While other isolated resonance windows at higher q_{95} have also been observed, the one at 3.7 has consistently produced good suppression results. Variations made during experiments in the reference shape also demonstrate that changes in, *e.g.*, triangularity, squareness, up-down symmetry, etc., have a significant impact on both the duration of the ELM suppression phase and the magnitude of the impulse reductions obtainable. The ITER shape [as shown in Fig. 2(b)] is of particular interest with respect to this question. While the pedestal profile parameters expected in ITER (e.g., β, $\rho*$, ν) clearly cannot be obtained in DIII–D, the flux surface shape has been exactly reproduced in these experiments and good Type-I ELM suppression, qualitatively equivalent to those found in the reference shape, has been achieved. An example of this is shown in Fig. 9 which can be compared with results from the reference shape shown in Fig. 4.

3. Discussion and Implications for Future Devices

It is difficult to extrapolate these results to other devices. Due to coil current limitations, we did not obtain a broad stochastic flux loss region in our best suppression case as originally envisioned. Vacuum field line integration modeling using the TRIP3D code [10] indicates that the best ELM suppression occurs when a weak stochastic magnetic layer is formed across most of the pedestal with a narrow poloidal flux loss region (~3% in ψ_n) at the foot of the pedestal and a relatively large (~3–4% in ψ_n) island chain on the q=3 surface at the top of the pedestal [8]. The lack of a wide stochastic flux loss region in the TRIP3D modeling is consistent with the observed lack of change to the electron pedestal profiles. Further, the lack of any measurable change in any diagnostics when the same external perturbation is applied in L–mode suggests that the TRIP3D modeling is incomplete because the plasma response in H–mode is critical for obtaining ELM suppression. There is also evidence that the ELM behavior depends on the mixing of the applied external perturbation with the intrinsic field

errors in DIII–D, and it is difficult to predict the spectrum and amplitude of such field errors in future devices. In fact, the sensitivity of the observed ELM behavior to the toroidal phase of the externally applied $n=3$ perturbation field relative to the intrinsic field errors suggests that differences in ELM behavior between devices might arise from differences in the intrinsic errors in those devices. We also note that even in the best suppression cases, we always observe a few isolated ELM-like events. The characteristics of these events are still under investigation. In some cases, they produce very small drops in the plasma stored energy while in others they produce drops in stored energy equivalent to or slightly exceeding those of a typical Type-I ELM. It seems plausible to assume that if the higher frequency transport induced by the magnetic perturbation is not of sufficient magnitude to maintain a balance between the core energy production rate and power exhaust through the boundary, a net accumulation will occur and result in impulses equivalent to those of Type-I ELMs.

An equally important consideration for applying this approach to future devices is the relatively narrow resonant window observed during these experiments. Because the I-coil was not designed with edge stochastic layer control applications in mind, its spectrum is not particularly well suited for this task. In principle, the narrowness of the resonance window can be expanded by introducing a denser mode spectrum across the pedestal and increasing the current capacity of the coil set. Future experiments, utilizing the full 7 kA current carrying capability of the DIII–D I-coil, will provide key information on the relative importance of remnant island versus stochastic layer effects and on the effectiveness of increasing the coil current on broadening the resonant ELM suppression window.

4. Conclusions

Fast heat pulses, driven by large Type-I ELMs in the DIII–D divertor, are essentially eliminated for periods approaching 7 energy confinement times with small d.c. currents driven in a simple magnetic perturbation coil (the DIII–D I-coil). The amplitude of the currents required to eliminate all but a few isolated ELM-like impulses during an I-coil pulse is less than 0.4% of I_p. Based on vacuum field line modeling, the magnetic perturbation from the coil resonates strongly with the plasma flux surfaces across most of the pedestal region $0.9 \leq \psi_N \leq 1.0$ creating remnant islands surrounded by weakly stochastic field lines. The stored energy, β_N and H–mode quality factor are unaffected by the perturbation field. The electron pressure profile, radial electric field and poloidal rotation across the pedestal are also unaltered along with the H–mode transport barrier.

In the best suppression case, ELMs are replaced by an increase in electron density and magnetic field fluctuations. These fluctuations have a distinct bursty and/or intermittent character and are modulated by a 130 Hz oscillation with a 2 ms quiet period followed by a 6 ms active period. Using these values and estimates of the time required for the energy dump, implies roughly a factor of 3 reduction in the energy impulse source from the pedestal into the scarpe-off layer. The particle flux impulses to the divertor target are suppressed by about a factor of 3 within one ELM period by the I-coil perturbation. In addition, the heat flux to the divertor plate, as inferred from the surface temperature changes of the divertor tile near the strike point, becomes much less impulsive. The peak heat flux on the outer divertor target plates, averaged over many ELM periods, drops by at least a factor of 5.

Although ELM suppression is a resonant effect that depends on q_{95}, the shape/position of the plasma, the up-down symmetry and the toroidal phase of the applied perturbation, the use of larger coil current (up to the 7 kA I-coil design limit) will increase the resonant window and enable experiments with broader edge stochastic layers.

During suppression 5–15 kJ drops in the stored energy are observed less than half that normally observed during Type I ELMs (15–30 kJ).

Acknowledgments

Work supported by the U.S. Department of Energy under DE-FC02-04ER54698, DE-FG02-04ER54158, DE-AC04-94AL85000, W-7405-ENG-48, DE-FG02-89ER53297, DE-FG03-01ER54615, DE-AC05-00OR22725.

This work was performed under the auspices of the U.S. Department of Energy by the University of California, Lawrence Livermore National Laboratory under Contract W-7405-Eng-48.

References

[1] LOARTE, A., et al., Plasma Phys. Control. Fusion **44** (2002) 1815; LOARTE, A., et al., Plasma Phys. Control. Fusion **45** (2003) 1549.
[2] FEDERICI, G., et al., J. Nucl. Mater. **313-316** (2003) 11; FEDERICI, G., et al., Plasma Phys. Control. Fusion **45** (2003) 1523.
[3] PACHER, H.D., ITER Design Description Document ITER No. G 17 DDD 1 96-08-21 W2.1 Appendix E9, Section 1.7 (1996).
[4] MADDISON, G.P., et al., Plasma Phys. Control. Fusion **45** (2003) 1657.
[5] LANG, P.T., et al., Nucl. Fusion **43** (2003) 1110.
[6] TAMAI, H., et al., J. Nucl. Mater. **220-222** (1994) 365.
[7] FIELDING, S.J., et al., Controlled Fusion and Plasma Physics (Proc. 28th EPS Conf. Madeira, 2001), Vol. 25A, European Physical Society (2002) 1825.
[8] EVANS, T.E., et al., Phys. Rev. Lett. **92** (2004) 235003-1.
[9] EVANS, T.E., et al., "Suppression of large edge localized modes in high confinement DIII–D plasmas with a stochastic magnetic boundary", Plasma Surface Interactions (Proc. 16th Int. Conf. Portland, 2004) to be published in J. Nucl. Mater.
[10] EVANS, T.E., et al., Phys. Plasmas **3** (2002) 4957.
[11] JACKSON, G.L., et al., Controlled Fusion and Plasma Physics (Proc. 30th EPS Conf. St. Petersburg, 2003) CD-ROM P-4.47.
[12] EVANS, T.E., and MOYER, R.A., J. Nucl. Mater. **313-316** (2003) 1282.
[13] GRIBOV, Y., Physics Unit, ITER Naka Joint Work Site, Japan, personal communication.